Full path Trajectory Optimization for different constraints

AbdelMageed Mahmoud

***Abstract*—Most of previous work discussed about trajectory optimization for one phase either ascent or gliding. This paper introduced the full trajectory optimization for different vehicle dynamics, and how be linked these two dynamics in one optimal trajectory. The full path optimal trajectory is important for many applications like aerospace industry, computing rocket and missile launch trajectories. Another goal in the paper how to set the final constraints for the ascent phase to meet the initial requirements for gliding phase. Finally, full analysis for different final constraints at gliding phase was done to improve the algorithm and to be sure, it is suitable for different constraint problems.**

***Keywords*— Trajectory optimization, optimal control, Multi constraints nonlinear programming**

I. Introduction

Trajectory optimization has been a topic of considerable research of launch vehicles for over 40 years in practical engineering application where the optimal control theory is commonly applied to obtain optimal solutions. "The objective of an optimal control problem is to determine the control signals that will cause a process to satisfy the physical constraints and at the same time minimize (or maximize) some performance index" As defined by Kirk. Possible performance indices include time, fuel consumption, or any other parameter of interest in a given application [1, 2].

Trajectory optimization of the hypersonic vehicle is a difficult problem due to various constraints of thermal load, total load, and dynamic pressure. Numerous researches are being carried out in this field. Lin Ma, Zhijiang Shao, Weifeng Chen, Xinguang Lv and Zhengyu Song have optimized the problem of fuel-optimal lunar ascent phase using constant-thrust propulsion [3]. Tawifiqur Rahman, Zhou Hao used Legendre and Gauss pseudospectral methods to optimize the trajectory problem of a hypersonic vehicle [4]. Fariba Fahroo and I. Michael Ross solved the problem of Bolza arising in Trajectory Optimization [5]. Michael A. Paluszek and Stephanie J. Thomas compared three different global indirect approaches for solving the problem of finding optimal trajectories for low-thrust spacecraft [6]. Numerical algorithms for trajectory optimization for flight vehicles are currently studied. Huang GuoQiang, Lu YuPing, and Nan-Ying summarized the basic principle, characteristics, and application for all kinds of current trajectory optimization algorithms [7].

AbdelMageed Mahmoud is with Beihang University, School of Astronautics , Beijing, China, Email: a_mageid@hotmail.com

One of the most general solutions to the optimal control problems is the calculus of variations and Pontryagin's maximum principle. By applying these methods determine the first order necessary conditions for a solution, these necessary conditions reduce the optimal control problem to a two-point boundary value problem. For most problems, the boundary value problem is difficult to solve analytically, so numerical techniques are used to determine an approximation to the continuous problem. Numerical methods fall into Direct and Indirect methods [8].

Some of the Indirect methods are multiple shooting, quasi-linearization, and collocation which approximating the solution to the continuous necessary conditions. The advantages of indirect methods are the high accuracy and emphasis the solution satisfies the necessary optimality conditions. The disadvantage that the necessary optimality conditions must be derived analytically, the convergence is small, so a good initial guess is required and also a guess is required for costate, finally for path constrained problems the constrained and unconstrained arcs should know a priori [9].

Direct methods transcribe the continuous optimal control problem into a Nonlinear Programming Problem (NLP), which can be solved by well-developed algorithms. One of the most advantages the optimality conditions do not need to be derived, large radius of convergence, no need for a guess of the costates and finally the switching structure does not need to be known.

Another approach based on spectral methods used to parameterize both the states and controls. Piecewise polynomials used to approximate the differential equations at collocation points, states and controls can also be parametrized using global polynomials which typically have faster convergence rates than traditional methods. This method provides accurate state and control approximations.

Spectral methods were applied to optimal control problems using Chebyshev polynomials and then developed the Legendre pseudospectral method using Lagrange polynomials and collocation at Legendre-Gauss-Lobatto (LGL) points. Finally, Gauss Pseudospectral Method (GPM) has been shown to satisfy the optimality conditions for a large class of problems [8, 10].

GPM proved an efficient way to solve the trajectory optimization problem, and besides it has high precision and fast rate of convergence, it equivalences the Karush-Kuhn-Tucker (KKT) condition and the Hamiltonian Boundary Value Problem (HBVP).

Full path trajectory optimization is very important in the field of a ballistic missile to get the optimal trajectory and optimal control along the full path many types of research

discussed the ascent phase and reentry phase separately, but a few discuss the full path.

For ascent phase, H. Xu and WanchunChen [11] provide the ascent guidance of solid-rocket-powered launch vehicles subject to the terminal velocity, terminal local flight path angle, and terminal angle of attack constraints. Da Zhang, Xuefang Lu, L. Liu, and Y. Wang [12] described an online reconstruction algorithm using Gauss Pseudospectral method to ascent phase trajectory. P. Lu, L. Zhang, and H. Sun [13] developed methodology and algorithms for on-demand generation of optimal launch vehicle ascent trajectories from lift-off to achieving targeting condition outside the atmosphere. G. Dukeman [14] developed an algorithm which solved the calculus-of-variations two-point boundary value problem starting at vertical rise completion through main engine cutoff, taking into account atmospheric effects.

For reentry phase K. Z. a. W. Chen [15] proposed two examples for optimization implementation using Easy Gauss pseudospectral method EGPM in the paper, first is maximum downrange without path constraints during the second multi-phase trajectory satisfying waypoint and a no-fly zone. P. Lu [16] developed predictor-corrector reentry algorithm for inequality constraint which met the appropriate augmentations of altitude rate feedback. The method successfully applied to three very different vehicles, a capsule, a shuttle class vehicle, and a high-lifting hypersonic gliding vehicle. Z. Hao, L. Jiafeng, C. Wanchun, and T. Rahman [17] provided reentry trajectory optimization phase, divided the reentry phase into two phases descent phase and glide phase. In descent phase, the angle of attack is set to fit the glide condition with the path constraints while in glide phase the attitude-velocity profile designed to maintain the safe flight corridor.

For full path trajectory optimization, M. H. Gräßlin, J. Telaar, and U. M. Schöttle [18] proposed NonLinear Programming (NLB) based on guidance strategies on autonomy, accuracy and mission flexibility for the ascent flight of the reusable launch vehicle Hopper during the space plane X-38 for reentry.

This paper describes full path trajectory optimization with multiple constraints using Gauss Pseudospectral method and how the full path trajectory divided into ascent phase and reentry phase. In ascent phase, the trajectory divided into 4 phases to get smooth and continuous control variable which it will be square the derivative of the angle of attack. Then the terminal point for the ascent phase will be the initial point for reentry phase. For reentry phase how to satisfy the terminal constraints, the control variables will be the sum of the square of the derivatives of the angle of attack and bank angle and finally the linkage between these two phases to get the full path trajectory optimization.

II. Ascent Vehicle Model

For the ascent phase 3-DOF kinematic model used for describing the vehicle dynamics without considering the earth rotation as follows [19]:

$$\dot{x} = v\cos(\gamma) \tag{1}$$

$$\dot{h} = v\sin(\gamma) \tag{2}$$

$$\dot{v} = \frac{T\cos(\alpha) - D}{m} - g\sin(\gamma) \tag{3}$$

$$\dot{\gamma} = \frac{T\sin(\alpha) + L}{mv} - \frac{g}{v}\cos(\gamma) + \frac{v}{r}\cos(\gamma) \tag{4}$$

$$\dot{m} = -\frac{T}{I_{sp}\, g_0} \tag{5}$$

Where x, h is the down range and height respectively, v is the velocity vector, α is the angle of attack, γ are the flight path angle and m is the mass, T is the thrust vector, g is the gravitational force. D, L is the drag and lift force and are given as [20]:

$$D = \frac{1}{2}\rho v^2 S_{ref}\, C_D(M_a, \alpha) \tag{6}$$

$$L = \frac{1}{2}\rho v^2 S_{ref}\, C_L(M_a, \alpha) \tag{7}$$

Where (ρ, S_{ref}) are the air density of the current altitude and the reference area, respectively, C_L and C_D are the lift and drag coefficients, respectively, which are the non-linear functions of the attack α angle and the Mach M_a.

TABLE I. Initial and final conditions for ascent phase

Parameter	Symbol	value	Symbol	value
Downrange	x_0	$0\ m$	x_f	Free
Height	h_0	$2\ m$	h_f	$70000\ m$
Velocity	v_0	$30\ m/s$	v_f	Free
Flight path angle	γ_0	90°	γ_f	0°
Mass	m_0	$154200\ Kg$	m_f	Free
Angle of attack	α_0	0°	α_0	0°

For the ascent trajectory, the control variable chosen as the derivative of the angle of attack where the initial and final conditions for the ascent phase listed in Table 1. The performance index is the weighted square of the derivative of the angle of attack in stage 2 and stage 4 only because of the angle of attack set as zero in other stages during the ascent phase.

$$J = \int K_1\dot{\alpha}_2^2 + K_2\dot{\alpha}_4^2\ dt \tag{8}$$

So the final height is set to be constrained at specific altitude to be the initial condition for the reentry phase, also to reach suitable velocity acceptable for the reentry phase and

final flight path angle and angle of attack set to be zero at the end of the ascent phase.

All the final conditions used as initial conditions for the linkage between the ascent and reentry phase. The linkage between the Stages in the ascent phases will as follows

Linkage Constraints between the four phases in the ascent phase considered as:

The initial state, time of phase 2 and the final state, time of phase 1 are the same

$$x_0\{2\} - x_f\{1\}, t_0\{2\} - t_f\{1\} = 0 \quad (9)$$

The velocity constraint at phase 2 grows up to $M = 0.7 \sim 0.8$, and the angle of attack is negative.

$$v_f\{2\} - \ 0.8 * 325 = 0 \quad (10)$$

The initial state, time of phase 3 and the final state, time of phase 2 are the same

$$x_0\{3\} - x_f\{2\}, t_0\{3\} - t_f\{2\} = 0 \quad (11)$$

The initial state, time of phase 4 and the final state, time of phase 3 are the same

$$x_0\{4\} - x_f\{3\}, t_0\{4\} - t_f\{3\} = 0 \quad (12)$$

The results of the optimized ascent trajectory using pseudospectral method GPOPSII, part one should start vertically (Vertical flight phase) from $0 \sim t_1$ moreover, constraint the angle of attack set to be zero in this phase for a safe launch.

Then the turning flight started from $t_1 \sim t_3$ Which is the end of phase three, during these two phases (phases 2 and 3) the hypersonic vehicle completed its rotation. In part 2 the velocity constraint grows up until Mach reaches between $0.7 \sim 0.8$ and angle of attack should be negative within 3 degrees.

Finally, part four satisfies the terminal conditions for the ascent phase through the final height, flight path angle and angle of attack.

To consider the states differential equations for the glide phase, we should convert the previous equations to the 3-D dynamics equation by adding static parameter ψ to the state equations of ascent phase as follows:

$$M_x = \begin{bmatrix} 1 & 0 & 0 \\ 0 & \cos\left(\frac{\pi}{2} - \text{lat}\right) & \sin\left(\frac{\pi}{2} - \text{lat}\right) \\ 0 & -\sin\left(\frac{\pi}{2} - \text{lat}\right) & \cos\left(\frac{\pi}{2} - \text{lat}\right) \end{bmatrix} \quad (13)$$

$$M_z = \begin{bmatrix} \cos\left(\text{lon} + \frac{\pi}{2}\right) & \sin\left(\text{lon} + \frac{\pi}{2}\right) & 0 \\ -\sin\left(\text{lon} + \frac{\pi}{2}\right) & \cos\left(\text{lon} + \frac{\pi}{2}\right) & 0 \\ 0 & 0 & 1 \end{bmatrix} \quad (14)$$

Where lat is the latitude, lon is the longitude and the transformation matrix from space to ground C_{gs} moreover, its transpose C_{sg} calculated as follows;

$$C_{gs} = M_x * M_z \quad (15)$$

$$C_{sg} = C_{gs}' \quad (16)$$

Considering the radius of the earth $R = 6378145$ to calculate the position corresponding to the earth as a function of latitude and longitude then put them as a vector R_s as follows;

$$R_{x\_s} = R * \cos(\text{lat}) * \cos(\text{lon})$$

$$R_{y\_s} = R * \cos(\text{lat}) * \sin(\text{lon})$$

$$R_{z\_s} = R * \sin(\text{lat})$$

$$R_s = \begin{bmatrix} R_{x\_s} \\ R_{y\_s} \\ R_{z\_s} \end{bmatrix} \quad (17)$$

Where X_g is the position, and V_g is the velocity vectors on ground coordinates and calculated as follows;

$R_w = R * \cos(\text{lat}) * \text{Omega}$; Omega is the earth rotation

$$X_{xg} = x_f * \cos(\psi)$$

$$X_{yg} = x_f * \sin(\psi)$$

$$X_{zg} = y_f$$

$$X_g = \begin{bmatrix} X_{xg} \\ X_{yg} \\ X_{zg} \end{bmatrix} \quad (18)$$

Where V_g is the velocity vector on ground coordinates and calculated as follows;

$$V_{zg} = v_f * \sin(\text{gammaf})$$

$$V_{xg} = v_f * \cos(\text{gammaf}) * \cos(\psi) + R_w$$

$$V_{yg} = v_f * \cos(\text{gammaf}) * \sin(\psi)$$

$$V_g = \begin{bmatrix} V_{xg} \\ V_{yg} \\ V_{zg} \end{bmatrix} \quad (19)$$

Finally, the position and velocity vector r and v are calculated on space coordinates as follows;

$$r = C_{sg} * X_g + R_s \quad (20)$$

$$v = C_{sg} * V_g \quad (21)$$

There are some bounds for static parameter such as azimuth angle

$$\psi = \begin{cases} \text{lower bound} = 0 \\ \text{upper bound} = \text{pi} \end{cases}$$

At the end of this phase, optimized ascent trajectory calculated with achieving the terminal constraints which it will be the initial conditions for the following part (reentry part).

III. REENTRY VEHICLE MODEL

For reentry phase 3-DOF Common Aero-Vehicle (CAV) dynamics used over spherical and rotating earth used as follows [16, 21]:

$$\dot{r} = V\sin(\gamma) \tag{22}$$

$$\dot{\theta} = \frac{V\cos(\gamma)\sin(\psi)}{r\cos(\varphi)} \tag{23}$$

$$\dot{\varphi} = \frac{V\cos(\gamma)\cos(\psi)}{r} \tag{24}$$

$$\dot{V} = -\frac{D}{m} - g\sin(\gamma) + \omega^2 r\cos(\varphi)\left(\sin(\gamma)\cos(\varphi) - \cos(\gamma)\sin(\varphi)\cos(\psi)\right) \tag{25}$$

$$\dot{\gamma} = \frac{1}{V}\left(\frac{L\cos(\sigma)}{m} + \left(\frac{V^2}{r} - g\right)\cos(\gamma) + 2\omega V\cos(\varphi)\sin(\psi)\right) + \left(\omega^2 r\cos(\varphi)\left(\cos(\gamma)\cos(\varphi) + \sin(\gamma)\sin(\varphi)\cos(\psi)\right)\right) \tag{26}$$

$$\dot{\psi} = \frac{1}{V}\left(\frac{L\sin(\sigma)}{m\cos(\gamma)} + \frac{V^2}{r}\cos(\gamma)\sin(\psi)\tan(\varphi) - 2\omega V\left(\cos(\varphi)\tan(\gamma)\cos(\psi) - \sin(\varphi)\right)\right) + \left(\frac{\omega^2 r}{\cos(\gamma)}\sin(\varphi)\cos(\varphi)\sin(\psi)\right) \tag{27}$$

Where r is the radial distance, θ is the longitude, φ is the latitude. V is the relative earth velocity, γ is the flight path angle, ψ is the azimuth angle, m is the mass of the CAV vehicle, $g = \frac{\mu}{r^2}$ is the gravity acceleration where μ is earth's gravitational constant.

The aerodynamic forces acting on CAV vehicle as follows;

$$L = \frac{1}{2}\rho V^2 C_l S_{ref} \tag{28}$$

$$D = \frac{1}{2}\rho V^2 C_d S_{ref} \tag{29}$$

Where $\rho = \rho_0 \exp(-h/H)$ is the atmospheric density where ρ_0 is the standard atmospheric pressure from the sea level, h is the altitude. S_{ref} is the reference are for CAV vehicle. C_l and C_d are lift and drag coefficients, respectively.

There are two kinds of CAV, one of them is called AMaRV or CAV-L and the other HPMARV or CAV-H. The lift-to-drag ratio for CAV-L is 2.0-2.5 range while the lift-to-drag ratio for CAV-H is 3.5-5.0 range, CAV-H used for modeling the reentry trajectory optimization due to its ability for gliding without power through the atmosphere [22].

It assumed that the lift and drag coefficients dependent only on the angle of attack as follows:

$$C_l = k_{l1}\alpha + k_{l2} \tag{30}$$

$$C_d = k_{d1}\alpha^2 + k_{d2}\alpha + k_{d3} \tag{31}$$

Where $k_{l1} = 0.04675, k_{l2} = -0.10568, k_{d1} = 0.000508, k_{d2} = 0.004228$ and $k_{d3} = 0.0161$. The reference area of CAV-H is 0.4839 m^2. The mass of CAV-H is 907 Kg.

To suppress the oscillation in the reentry trajectory, we should keep the two-order derivative of flight path angle zero. So the command angle of attack and the bank angle used to calculate the proper flight path angle. The negative feedback signal defined as the deviation between the proper flight path angle and the actual flight path angle.

The special flight path angle γ_m calculated from command angle of attack and bank angle that keep the second-order derivative of flight path angle zero as follows [21];

$$\gamma_m = \frac{D}{-\frac{v^2 m}{H} - gm - \frac{2m^2v^2}{r^2} + \frac{2m^2 g}{r\rho c_L S_{ref}\cos(\sigma)} - \frac{2m^2 g^2}{v^2\rho c_L S_{ref}\cos(\sigma)}} + \frac{\dot{c}_L\cos(\sigma) - c_L\sin(\sigma)\,\dot{\sigma}}{\frac{vc_L\cos(\sigma)}{H} + \frac{gc_L\cos(\sigma)}{v} + \frac{2mv}{r^2\rho S_{ref}} - \frac{2mg}{r\rho v S_{ref}} + \frac{2mg^2}{r\rho v S_{ref}}} + \frac{D}{-\frac{r\rho v^2 c_L S_{ref}\cos(\sigma)}{2H} - \frac{rg\rho c_L S_{ref}\cos(\sigma)}{2} - \frac{mv^2}{r} + mg - \frac{mrg^2}{v^2}} + \frac{D}{-\frac{\rho v^4 c_L S_{ref}\cos(\sigma)}{2Hg} - \frac{v^2\rho c_L S_{ref}\cos(\sigma)}{2} - \frac{mv^4}{r^2 g} + \frac{mv^2}{r} - mg} \tag{32}$$

Where the lift coefficients and drag force used in the above equations calculated from the command angle of attack and bank angle. For the reentry trajectory, the control variables chosen as the derivative of the angle of attack and the bank angle.

Consider the following equations;

$$C_{l2}\cos(\sigma_2) = C_{l1}\cos(\sigma_1) + K(\gamma - \gamma_m) \quad (33)$$

$$C_{l2}\sin(\sigma_2) = C_{l1}\cos(\sigma_1) \quad (34)$$

Where C_{l2} is the actual lift coefficient and C_{l1} is the command lift coefficient. σ_2 is the actual bank angle while σ_1 is the command bank angle and K is the negative feedback gain.

So the actual angle of attack and bank angle can be calculated from the above equations as follows;

$$\sigma_2 = \tan^{-1}\left(\frac{C_{l1}\sin(\sigma_1)}{C_{l1}\cos(\sigma_1) + K(\gamma - \gamma_m)}\right) \quad (35)$$

$$\alpha_2 = \frac{1}{k_{l1}}\left(\frac{C_{l1}\cos(\sigma_1) + K(\gamma - \gamma_m)}{\cos(\sigma_2)} - k_{l2}\right) \quad (36)$$

Now rewrite the dynamics equation again but with integrating the trajectory-oscillation suppressing scheme that is mention above;

$$\dot{r} = V\sin(\gamma) \quad (37)$$

$$\dot{\theta} = \frac{V\cos(\gamma)\sin(\psi)}{r\cos(\varphi)} \quad (38)$$

$$\dot{\varphi} = \frac{V\cos(\gamma)\cos(\psi)}{r} \quad (39)$$

$$\dot{V} = -\frac{D_2}{m} - g\sin(\gamma) + \omega^2 r\cos(\varphi)\left(\sin(\gamma)\cos(\varphi) - \cos(\gamma)\sin(\varphi)\cos(\psi)\right) \quad (40)$$

$$\dot{\gamma} = \frac{1}{V}\left(\frac{L_2\cos(\sigma_2)}{m} + \left(\frac{V^2}{r} - g\right)\cos(\gamma) + 2\omega V\cos(\varphi)\sin(\psi)\right) + \left(\omega^2 r\cos(\varphi)\left(\cos(\gamma)\cos(\varphi) + \sin(\gamma)\sin(\varphi)\cos(\psi)\right)\right) \quad (41)$$

$$\dot{\psi} = \frac{1}{V}\left(\frac{L_2\sin(\sigma_2)}{m\cos(\gamma)} + \frac{V^2}{r}\cos(\gamma)\sin(\psi)\tan(\varphi) - 2\omega V(\cos(\varphi)\tan(\gamma)\cos(\psi) - \sin(\varphi))\right) + \left(\frac{\omega^2 r}{\cos(\gamma)}\sin(\varphi)\cos(\varphi)\sin(\psi)\right) \quad (42)$$

Where L_2 is the actual aerodynamic lift force.

The performance index chose to meet the requirements and constraints, also for smoothing the control parameter and the trajectory profile;

$$J = \int K_1\dot{\alpha}_1^2 + K_2\dot{\sigma}_1^2\, dt \quad (43)$$

Where K_1 and K_2 are controls weighting coefficients

TABLE II. INITIAL AND FINAL CONDITIONS FOR REENTRY PHASE

Parameter	Symbol	Initial value	Symbol	Final value
Radial distance	r_0	$Alt_0 + R_e$	r_f	$Alt_f + R_e$
Longitude	θ_0	0°	θ_f	Free
Latitude	φ_0	0°	φ_f	4°
Velocity	V_0	6900 m/s	V_f	2400 m/s
Flight path angle	γ_0	0°	γ_f	0°
Azimuth angle	ψ_0	65°	ψ_f	Free
Angle of attack	α_0	Free	α_0	Free
Bank angle	σ_0	Free	σ_f	Free

The initial condition for reentry phase listed in Table II as the initial altitude equal to $Alt_0 = 70000$ m, the initial longitude θ_0 moreover, initial latitude φ_0 equal to zero same as the initial flight path angle γ_0 while the initial velocity $V_0 = 6900$ m/s, initial azimuth angle $\psi_0 = 65°$. Finally the angle of attack α_0 moreover, bank angle σ_0 is set to be free.

While the terminal constraints set for the final altitude$\mathrm{Alt_f} = 30000$ m, final latitude $\varphi_f = 4°$, final velocity $\mathrm{V_f} = 2400$ m/s, final flight path angle $\gamma_f = 0°$, while the other states set to be free.

The results in this phase represent the states achieved the terminal constraints with the control variables angle of attack and bank angle smooth. Last part how to link the two phases to be full path trajectory that explained in the next part.

IV. Linkage between Ascent and reentry phases

In this section, we will discuss the full path optimized trajectory by linking the two phases with each other the ascent phase and the reentry phase. Also, discuss how to calculate the initial latitude and longitude for reentry phase from the position vector which is the end of the ascent phase and choose suitable performance index to make the control variables smooth and continues.

The initial latitude and longitude can be calculated from the position vector as follows;

$$\theta_0 = \tan^{-1}\left(\frac{Y_e}{X_e}\right) \tag{44}$$

$$\varphi_0 = \sin^{-1}\left(\frac{Z_e}{R}\right) \tag{45}$$

Where $(X_e \quad Y_e \quad Z_e)$ is the position vector, and $R = 6367449$ m is the radius of the earth.

Linkage Constraints between the ascent and reentry phases considered as:

The initial states, time of reentry phase and the final states, time of ascent phase are the same as follows;

Initial radial distance of the reentry phase will equal to the terminal height of the ascent phase plus earth radius

$$x_0\{5\}(1) - (x_f\{4\}(2) + R_e) = 0 \tag{46}$$

initial longitude of the reentry phase will equal to θ_0

$$x_0\{5\}(2) - \theta_0 = 0 \tag{47}$$

initial latitude of the reentry phase will equal to φ_0

$$x_0\{5\}(3) - \varphi_0 = 0 \tag{48}$$

the initial velocity of the reentry phase will equal to the terminal velocity of the ascent phase

$$x_0\{5\}(4) - x_f\{4\}(3) = 0 \tag{49}$$

initial flight path angle of the reentry phase will equal to the terminal flight path angle of the ascent phase

$$x_0\{5\}(5) - x_f\{4\}(4) = 0 \tag{50}$$

Initial azimuth angle of the reentry phase will equal to ψ_0 which is static parameter chose as

$$x_0\{5\}(6) - \psi_0 = 0 \tag{51}$$

Initial angle of attack of the reentry phase will equal to the terminal angle of attack of the ascent phase

$$x_0\{5\}(7) - x_f\{4\}(5) = 0 \tag{52}$$

Initial bank angle of the reentry phase will set to be free while initial time of the reentry phase will equal to the terminal time of the ascent phase

$$t_0\{5\} - t_f\{4\} = 0 \tag{53}$$

The performance index chose as the sum of weighting control variables squares in phase 2, phase 4 at scent phase and phase 5 at reentry phase to continuous and smoothing the control variables along the full path as follows;

$$J = \int K_1\dot{\alpha}_2^2 + K_2\dot{\alpha}_4^2 + K_3\dot{\alpha}_5^2 + K_4\dot{\beta}_5^2 \, dt \tag{54}$$

Where K_1, K_2, K_3, K_4 are weighting parameter for the performance index while $\dot{\alpha}_2^2, \dot{\alpha}_4^2$ are the square of the control variables for phase 2 and phase 4 at ascent phase while $\dot{\alpha}_5^2, \dot{\beta}_5^2$ are the square of the control variables on reentry phase.

V. Gauss PSEUDOSPECTRAL METHOD FORMULATION

The theory of GPM discussed in details by David Benson [10]. GPM transforms the optimal control problem into an NLP problem which is then solved using NLP solver. The principle of Gauss pseudospectral method discretizes the state and control variables of the dynamics equations at Legendre-Gauss (LG) points. Then differentiate the polynomials to approximate the derivative of the state variables and convert the differential equations to algebraic equations constraints. The integral parts of the cost function are approximated using the Gauss quadrature. The terminal states determined by the initial states and the Gauss quadrature. After the transcription above, the optimal control problems converted to nonlinear program problems with a series of algebraic equations constraints [8, 23].

$$J = \phi(x(-1), t_0, x(1), t_f) + \frac{t_f - t_0}{2}\int_{-1}^{1} g(x(\tau), u(\tau), \tau; t_0, t_f)\, d\tau \tag{55}$$

Subjected to:

$$\frac{dx}{d\tau} = \frac{t_f - t_0}{2} f(x(\tau), u(\tau), \tau; t_0, t_f) \tag{56}$$

$$\Phi(x(-1), t_0, x(1), t_f) = 0 \tag{57}$$

$$C(x(\tau), u(\tau), \tau; t_0, t_f) \leq 0 \tag{58}$$

Where $x(\tau) \in R^n, u(\tau) \in R^m$ are the state and control variables, respectively; t_0, t_f are the initial and final time, respectively. The optimal control problem for the above equations called continues Bolza problem where time variable $\tau \in [-1,1]$, $t \in [t_0, t_f]$ can be transformed by the following equation:

$$t = \frac{t_f - t_0}{2}\tau + \frac{t_f + t_0}{2} \tag{59}$$

Then the state variable and control variable discretized by using a basis of N+1 Lagrange interpolating polynomial $\mathcal{L}_i$ moreover, a basis of N Lagrange interpolating polynomial $\mathcal{L}_i^*$ then transcribed to a nonlinear programming problem.

$$x(\tau) \approx X(\tau) = \sum_{i=0}^{N} X(\tau_i)\mathcal{L}_i(\tau_i) \tag{60}$$

Where $\mathcal{L}_i(\tau)(i = 0, \dots \dots, N)$defined as:

$$\mathcal{L}_i(\tau) = \prod_{j=0, j\neq i}^{N} \frac{\tau - \tau_j}{\tau_i - \tau_j} \tag{61}$$

$$u(\tau) \approx U(\tau) = \sum_{i=1}^{N} U(\tau_i)\mathcal{L}_i^*(\tau_i) \tag{62}$$

$$\mathcal{L}_i^*(\tau) = \prod_{j=1, j\neq i}^{N} \frac{\tau - \tau_j}{\tau_i - \tau_j} \tag{63}$$

Equations (61) and (62) satisfy the properties

$$\mathcal{L}_i(\tau) = \begin{cases} 1, i = j \\ 0, i \neq j \end{cases} \tag{64}$$

$$\mathcal{L}_i^*(\tau) = \begin{cases} 1, i = j \\ 0, i \neq j \end{cases} \tag{65}$$

Differentiate the expression in Eq.(49)

$$\dot{x}(\tau) \approx \dot{X}(\tau) = \sum_{i=0}^{N} X(\tau_i)\dot{\mathcal{L}}_i(\tau_i) \tag{66}$$

The Differential approximation matrix $D \in R^{N\times N+1}$ gets the derivative of each Lagrange polynomial at Legendre-Gauss (LG) points as follows

$$D_{ki} = \dot{\mathcal{L}}_i(\tau_k) = \sum_{l=0}^{N} \frac{\prod_{j=0, j\neq i}^{N}(\tau_k - \tau_j)}{\prod_{j=0, j\neq i}^{N}(\tau_i - \tau_j)} \tag{67}$$

Where $k = 1, \dots, N$ and $i = 0, \dots . N$ the dynamic constraint is transcribed into algebraic constraints using the differential approximation matrix by;

$$\sum_{i=0}^{N} D_{ki}\, X_i - \frac{t_f - t_0}{2} f(x(\tau), u(\tau), \tau; t_0, t_f) = 0 (k = 1, \dots, N) \tag{68}$$

Where $X_k \equiv X(t_k) \in R^n$ and $U_k \equiv U(t_k) \in R^m (k = 1, \dots \dots, N)$. The dynamic constraint is collocated only at the LG points and not at the boundary points.

Additional variables in the discretization are defined as follows, $X_0 \equiv X(-1)$, and $X_f \equiv X(1)$ where X_f is defined via the Gauss quadrature:

$$X_f = X_0 + \frac{t_f - t_0}{2} \sum_{k=1}^{N} \omega_k\, f(x_k, u_k, \tau_k; t_0, t_f) \tag{69}$$

Where ω_k are the Gauss weights. The continuous cost function of Eq.(24) is approximated using a Gauss quadrature as

$$J = \phi(X_0, t_0, X_f, t_f) + \frac{t_f - t_0}{2} \sum_{k=1}^{N} \omega_k\, g(x_k, u_k, \tau_k; t_0, t_f) \tag{70}$$

Finally, the continuous Bolza optimal control problem discretized as follows:

$$\min\ J = \phi(X_0, t_0, X_f, t_f) + \tfrac{t_f - t_0}{2} \textstyle\sum_{k=1}^{N} \omega_k\, g(x_k, u_k, \tau_k; t_0, t_f)$$

$$\text{s.t.}\ \ \textstyle\sum_{i=0}^{N} D_{ki}\, X_i - \tfrac{t_f - t_0}{2} f(x(\tau), u(\tau), \tau; t_0, t_f) = 0$$

$$\Phi(X_0, t_0, X_f, t_f) = 0$$

$$C(x_k, u_k, \tau_k; t_0, t_f) \leq 0$$

VI. SIMULATION AND RESULTS

Trajectory optimization problem was solved using GPM. In GPM the problem was solved as a multiphase single trajectory problem using GPOPS® [24] where SNOPT® used as NLP solver.

The method presented above is applied in simulations to the full path trajectory optimization (ascent and reentry phases) with multi-constraints. For the ascent phase how to reach the terminal point that it will be the initial point for the reentry phase and also in the reentry phase how to achieve the terminal constraints and the linkage between the phases. The performance index for the ascent phase is the derivative of the angle of attack to control the profile of the angle of attack during the ascent phase while for the gilding phase the derivatives of the angle of attack and the bank angle used as control parameters.

The following figures show the variation for the different states for ascent and reentry phases. For ascent phase only include the downrange, mass. For full path trajectory include the remaining states, height, velocity, flight path angle, the angle of attack. There are other states begin the reentry phase like latitude, longitude, azimuth angle and bank angle.

Figures (1~2) describe the ascent phase only, Figure 1 represents the down-range which explains the downrange of the vehicle during ascent phase and figure 2 represents the mass profile explained the mass burning rate for the two stages.

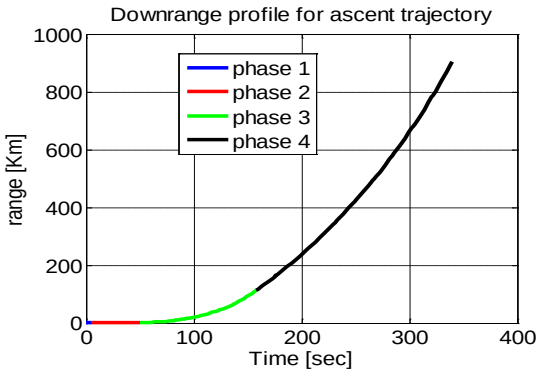

Figure 1 down range for ascent trajectory

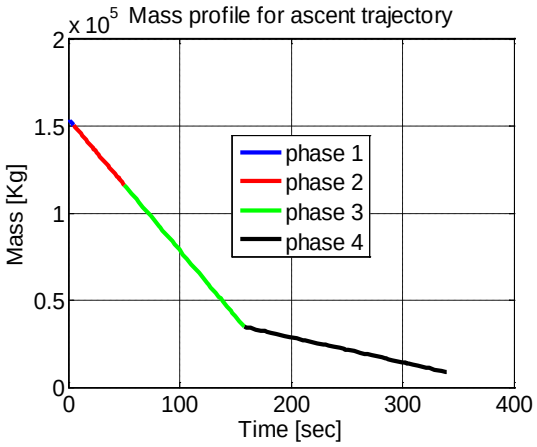

Figure 2 Mass profile for ascent trajectory

Figures (3~6) describes the full path trajectory optimization. Figure 3 represents the height which begins from the initial height till it reaches the terminal point (70,000 m) of the ascent phase which it will be the initial point for the reentry phase till it reaches the terminal point of the reentry phase(30,000 m). Figure 4 represents the velocity profile of full trajectory which begins from the initial velocity and reaches the terminal point of the ascent phase (7000 m/s) which it will be the initial point for the reentry phase till it reaches the terminal point for the reentry phase (2400 m/s). Figure 5 represents the flight path angle of full path trajectory which begins from $90°$ vertically and then decreases until it reaches zero at the end of the ascent phase, also continue around zero between $(-1°\sim1°)$ at the reentry phase. Finally, figure 6 for the control variable angle of attack of full path trajectory at ascent phase. This phase divided into 4 phases, the first phase it begins zero and then the second phase decreases for maximum $-5°$ then third phase increases again to zero for the last phase in ascent it increases to be the initial point for reentry phase which it is constant in the reentry phase.

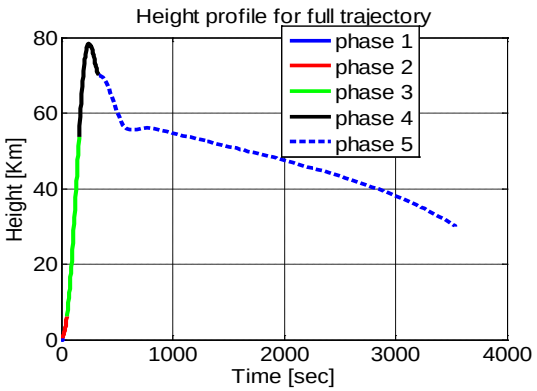

Figure 3 Height profile for full trajectory

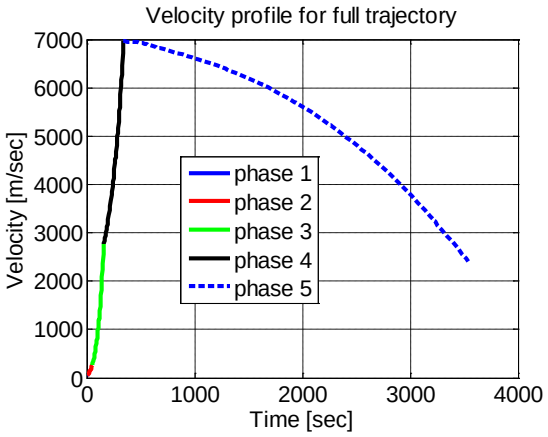

Figure 4 Velocity profile for full trajectory

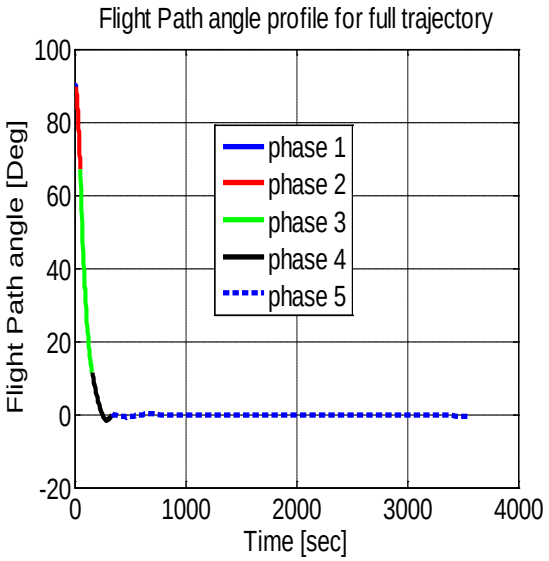

Figure 5 Flight path angle for full trajectory

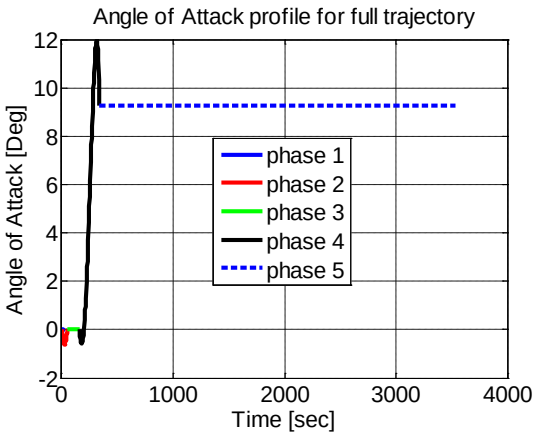

Figure 6 Angle of attack for full trajectory

Figures (7~10) describes the reentry phase only for latitude, longitude, azimuth angle and bank angle. Figure 7 represents the azimuth angle for reentry phase where its static parameter for the program and its initial point chose to meet the constraints, and its terminal point is free. Figure 8 represents the bank angle where it is the second control variable for reentry phase, initial and terminal points are free, and its deviations are little small. Figures (9~10) represents the latitude and longitude respectively, for their initial points calculated from the position vector of the terminal point of the ascent phase while the terminal point for latitude fixed as terminal constrained for reentry phase equal to 4° while the terminal point for longitude is free.

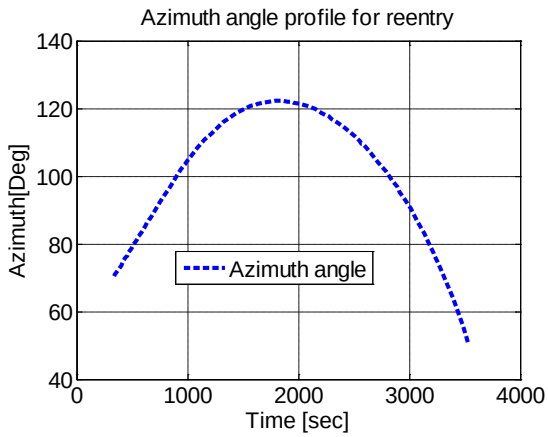

Figure 7 Azimuth angle profile for reentry phase

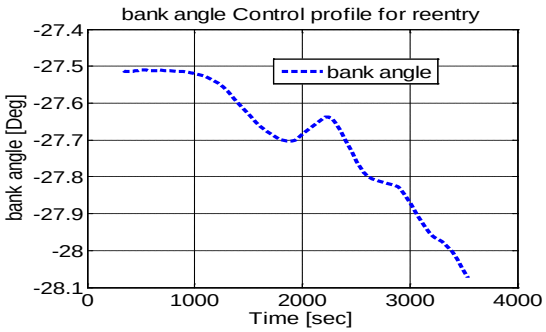

Figure 8 bank angle for reentry phase

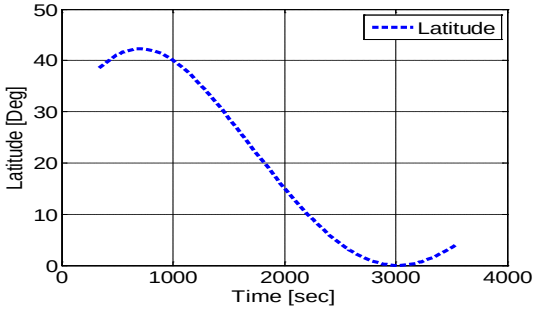

Figure 9 Latitude profile for reentry phase

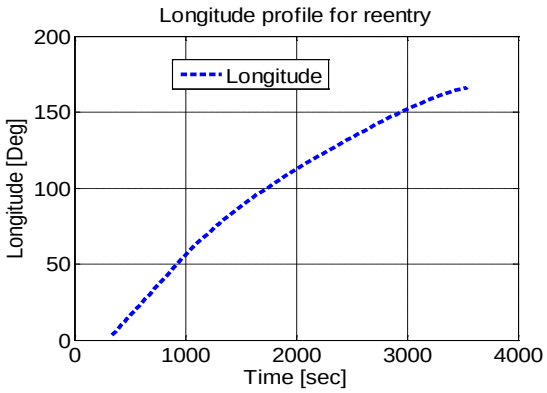

Figure 10 Longitude profile for reentry phase

VII. Second Case Study for Max Latitude

The objective function in second case study is max latitude at the reentry phase for full trajectory without suppressing the oscillations in the range profile; the next Table 1 represents the different constraints at the initial and final points

Table 1 Initial and Final constraints for max latitude

Parameter	Symbol	Initial value	Symbol	Final value
Height	r_0	70000 m	r_f	30000 m

Parameter	Symbol	Initial value	Symbol	Final value
Longitude	θ_0	0°	θ_f	Free
Latitude	φ_0	0°	$\boldsymbol{\varphi_f}$	**Max**
Velocity	V_0	6900 m/s	V_f	2400 m /s
Flight path angle	γ_0	0°	γ_f	0°
Azimuth angle	ψ_0	65°	ψ_f	Free
Angle of attack	α_0	Free	α_0	Free
Bank angle	σ_0	Free	σ_f	Free

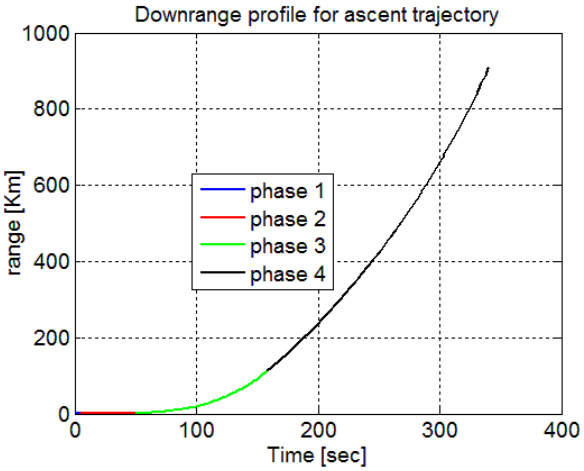

Figure 11 downrange profile for max latitude

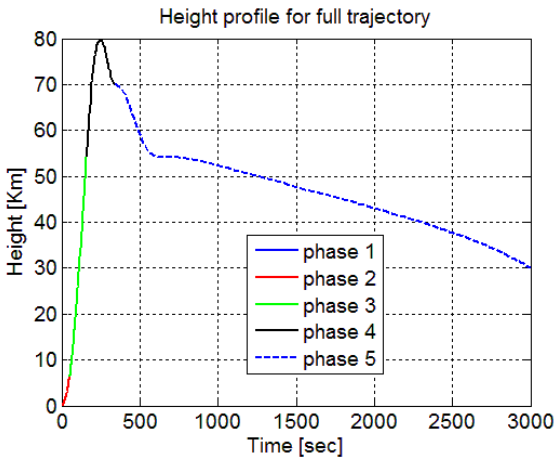

Figure 12 Height profile for max latitude

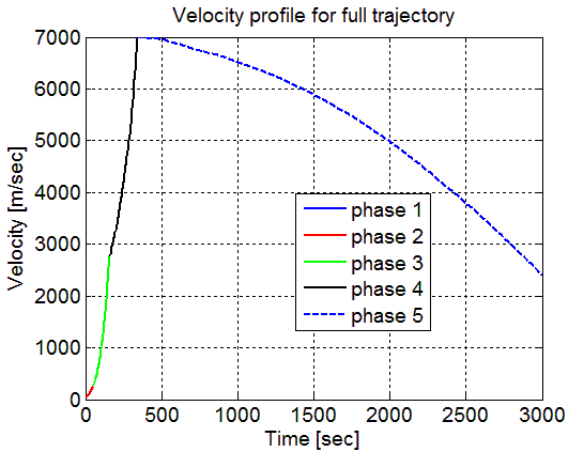

Figure 13 Velocity profile for max latitude

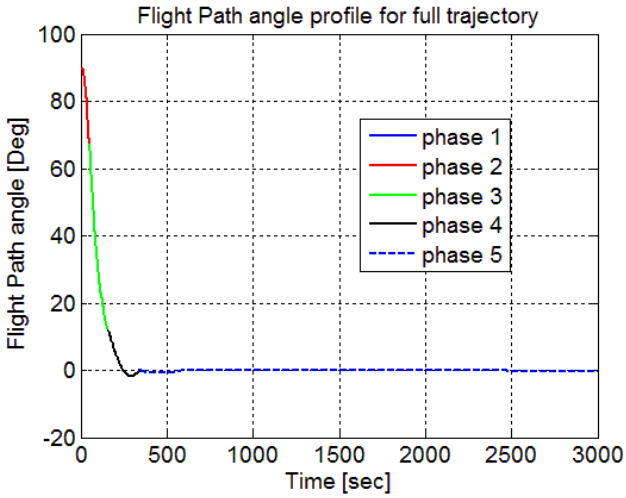

Figure 14 Flight path angle profile for max latitude

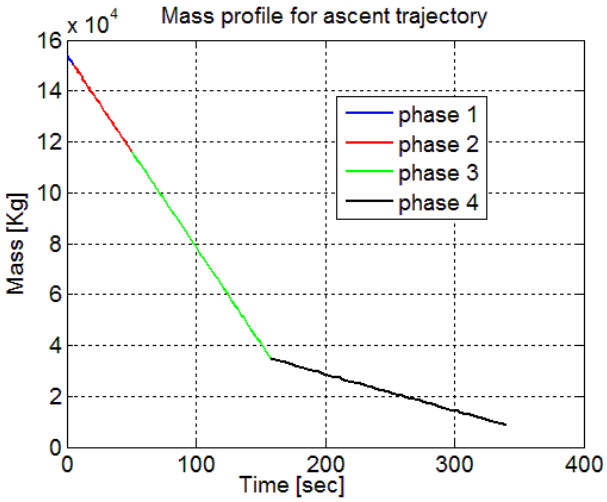

Figure 15 Mass profile for max latitude

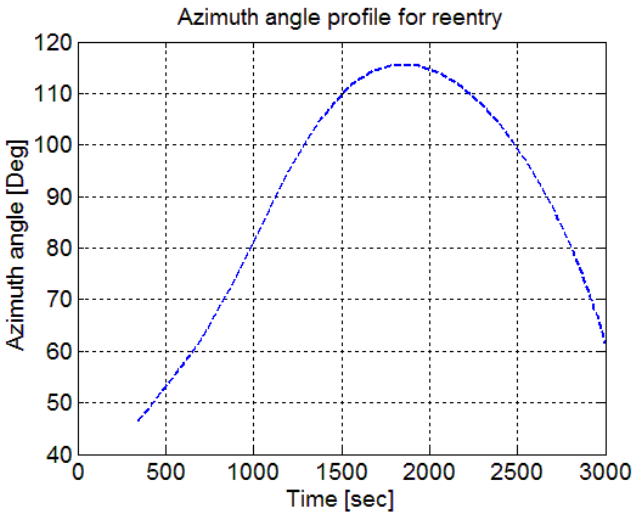

Figure 16 Azimuth angle profile for max latitude

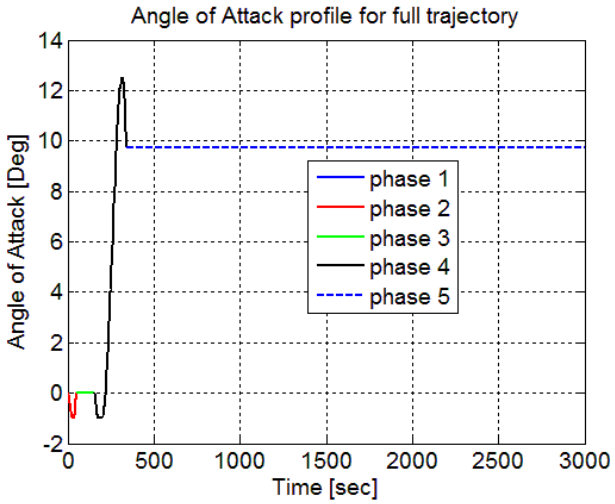

Figure 17 Angle of attack profile for max latitude

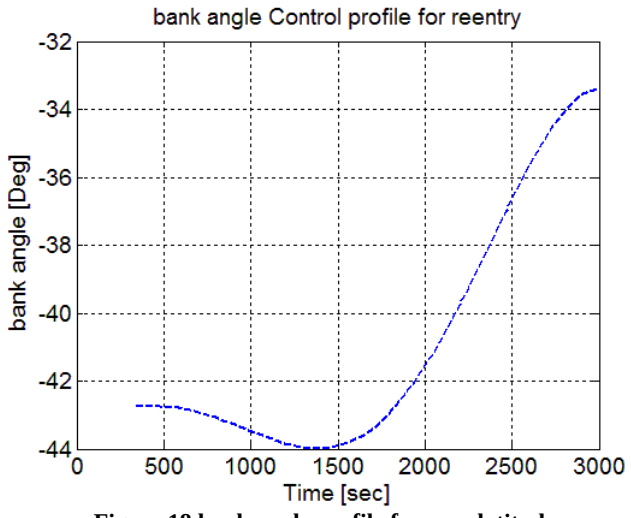

Figure 18 bank angle profile for max latitude

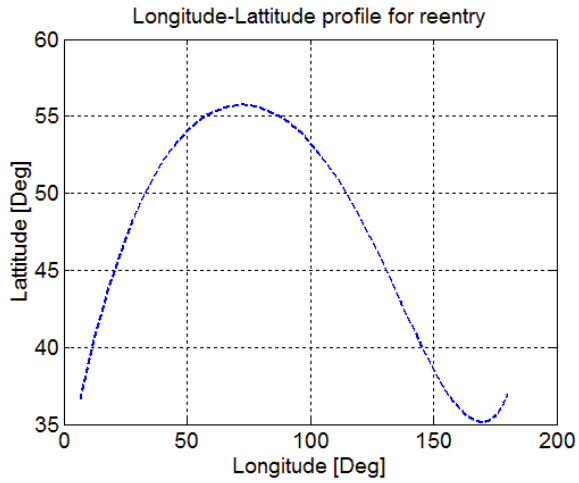

Figure 19 Longitude-Latitude profile for max latitude

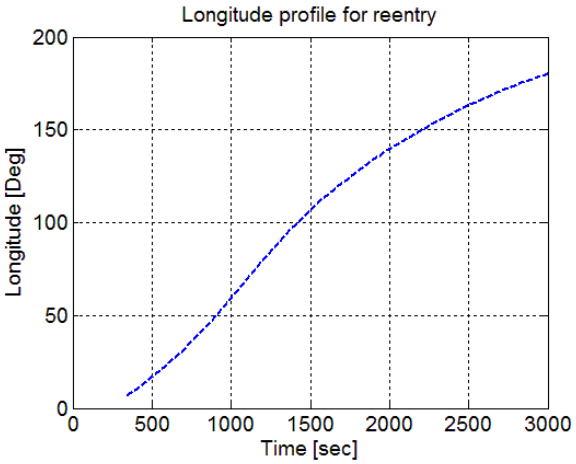

Figure 20 Longitude profile for max latitude

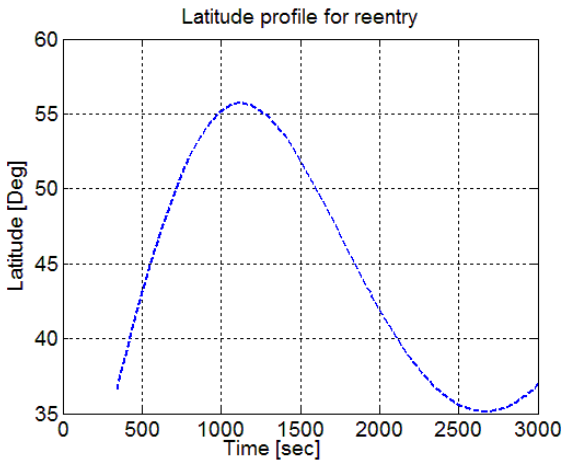

Figure 21 Latitude profile for max latitude

VIII. Third Case Study for Max Longitude

The objective function in third case study is max longitude at the reentry phase for full trajectory with suppressing the oscillations in the range profile; the next Table 2 represents the different constraints at the initial and final points

Table 2 Initial and Final constraints for max longitude

Parameter	Symbol	Initial value	Symbol	Final value
Height	r_0	70000 m	r_f	30000 m
Longitude	θ_0	0°	θ_f	Max
Latitude	φ_0	0°	φ_f	Free
Velocity	V_0	6900 m/s	V_f	2400 m/s
Flight path angle	γ_0	0°	γ_f	0°
Azimuth angle	ψ_0	65°	ψ_f	Free
Angle of attack	α_0	Free	α_0	Free
Bank angle	σ_0	Free	σ_f	Free

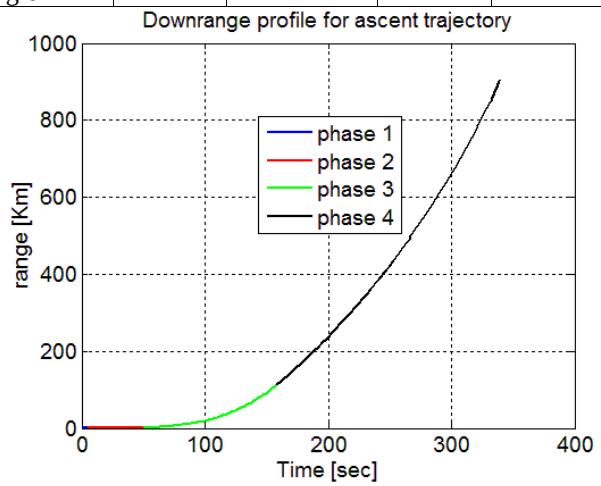

Figure 22 Range profile for full path trajectory

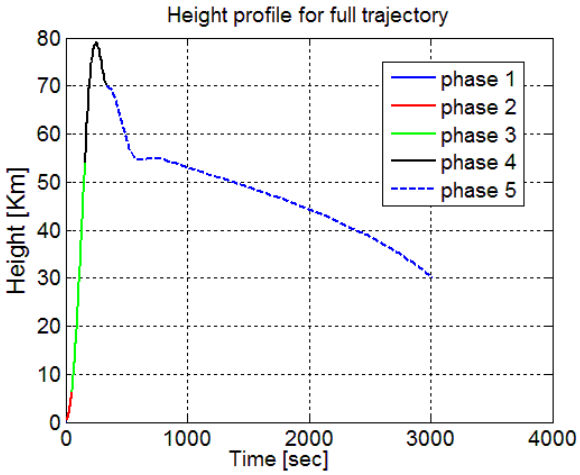

Figure 23 Height profile for full path trajectory

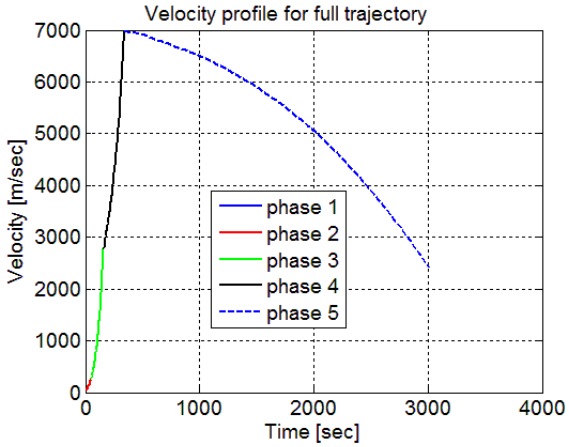

Figure 24 Velocity profile for full path trajectory

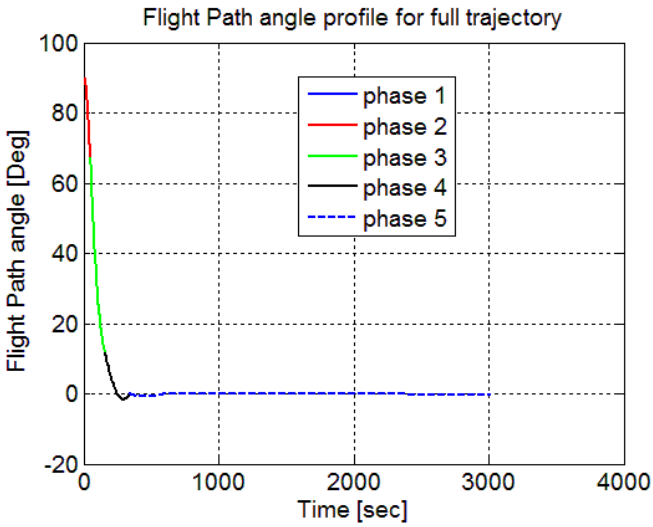

Figure 25 Flight path angle profile for full path trajectory

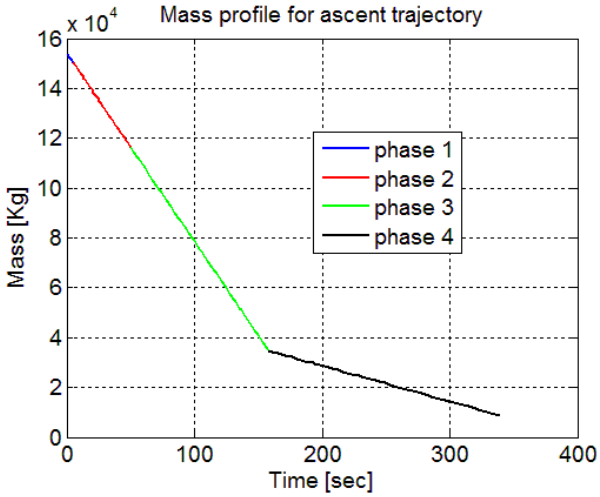

Figure 26 Mass profile for full path trajectory

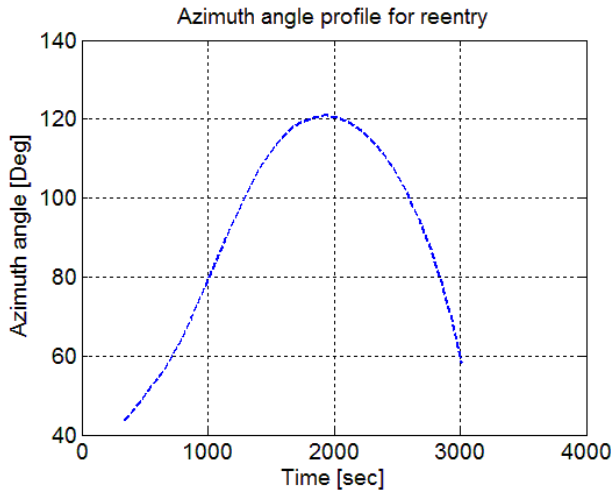

Figure 27 Azimuth profile for full path trajectory

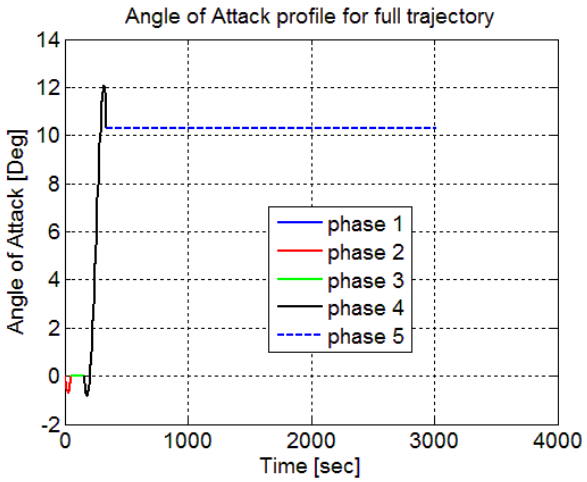

Figure 28 Angle of Attack profile for full path trajectory

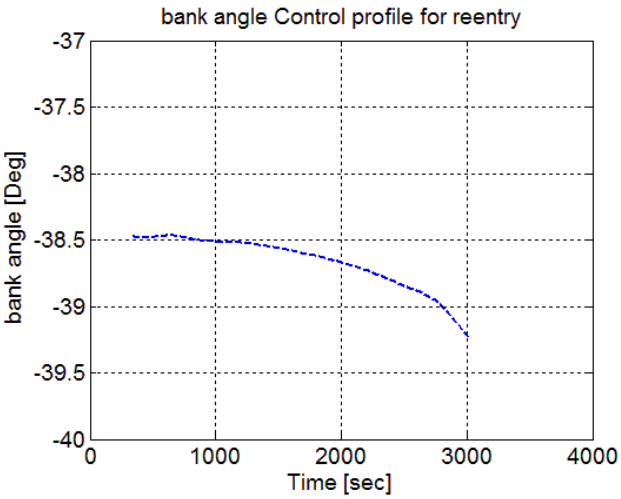

Figure 29 Angle of Attack profile for full path trajectory

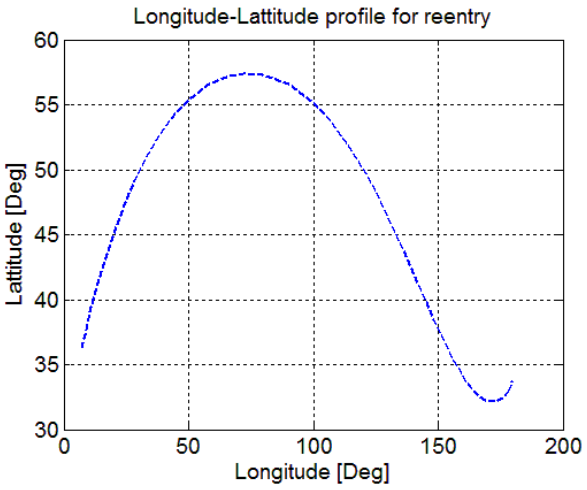

Figure 30 Longitude-Latitude profile for full path trajectory

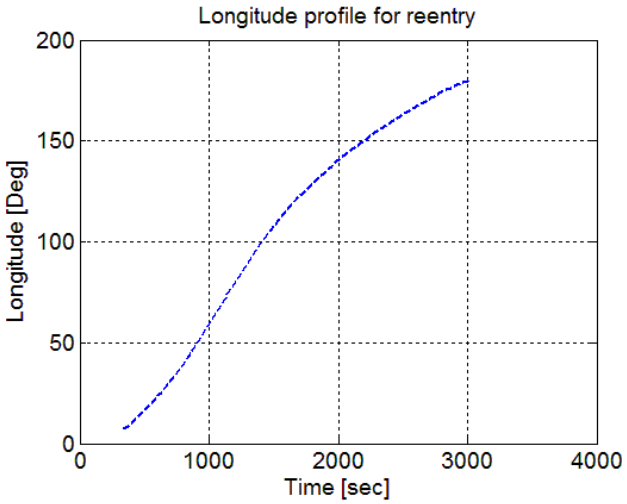

Figure 31 Longitude profile for full path trajectory

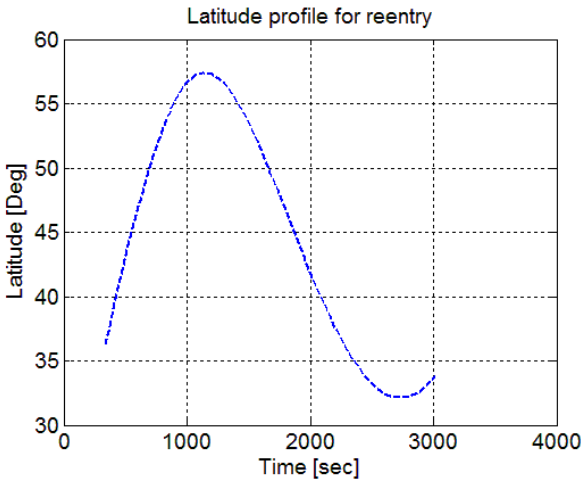

Figure 32 Latitude profile for full path trajectory

IX. Fourth Case Study for max Velocity

The objective function in Fourth case study is max velocity at the reentry phase for full trajectory with suppressing the oscillations in the range profile; the next Table 3 represents the different constraints at the initial and final points

Table 3 Initial and Final constraints for max velocity

Parameter	Symbol	Initial value	Symbol	Final value
Height	r_0	70000 m	r_f	Free
Longitude	θ_0	0°	θ_f	Free
Latitude	φ_0	0°	φ_f	4°
Velocity	V_0	6900 m/s	$\mathbf{V_f}$	**Max**
Flight path angle	γ_0	0°	γ_f	0°
Azimuth angle	ψ_0	65°	ψ_f	Free
Angle of attack	α_0	Free	α_0	Free
Bank angle	σ_0	Free	σ_f	Free

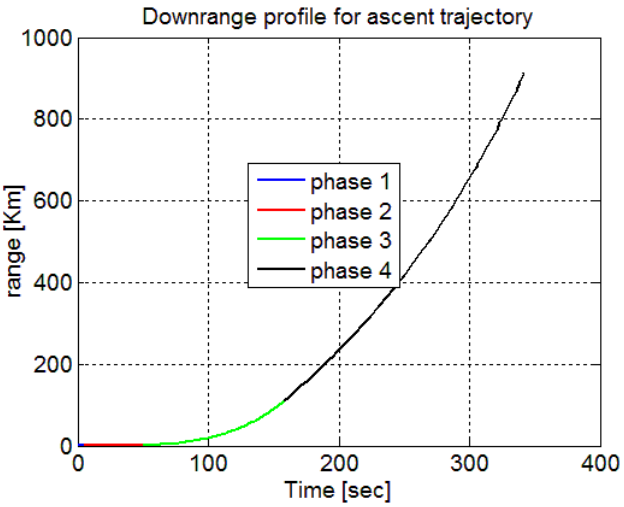

Figure 33 Range profile for full path trajectory

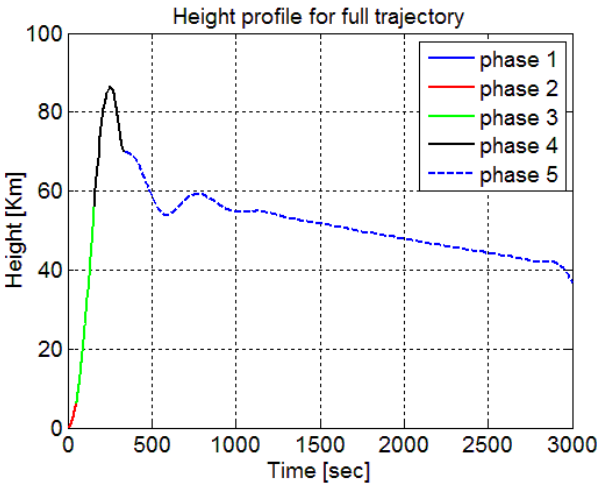

Figure 34 Height profile for full path trajectory

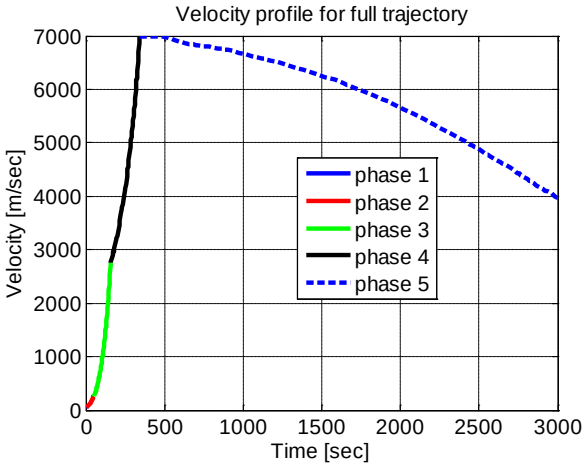

Figure 35 Velocity profile for full path trajectory

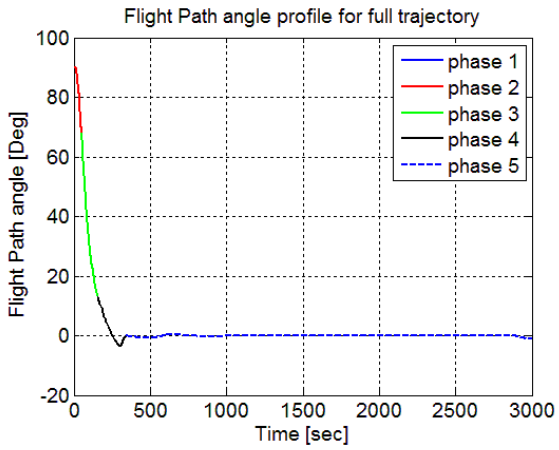

Figure 36 Flight path angle profile for full path trajectory

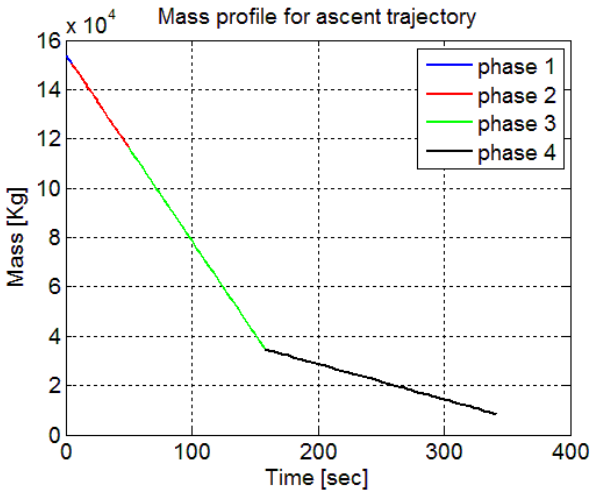

Figure 37 Mass profile for full path trajectory

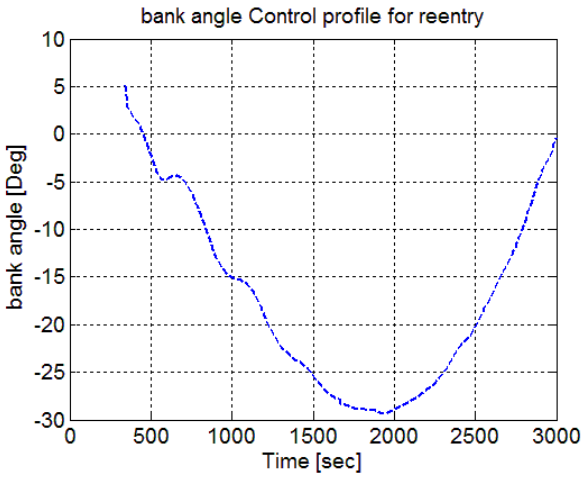

Figure 40 Bank angle profile for full path trajectory

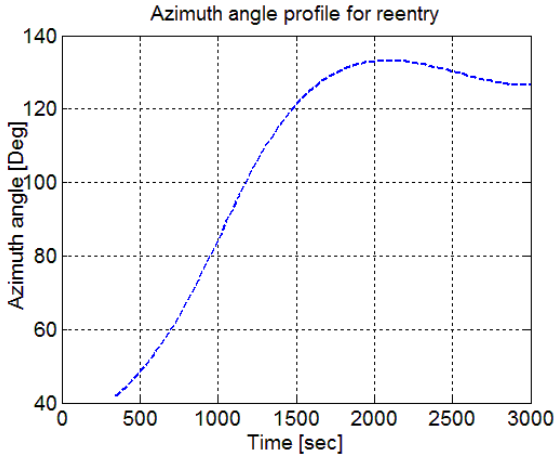

Figure 38 Azimuth Angle profile for full path trajectory

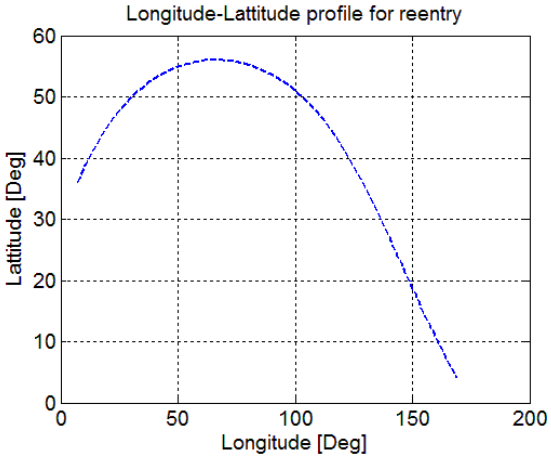

Figure 41 Longitude-Latitude profile for full path trajectory

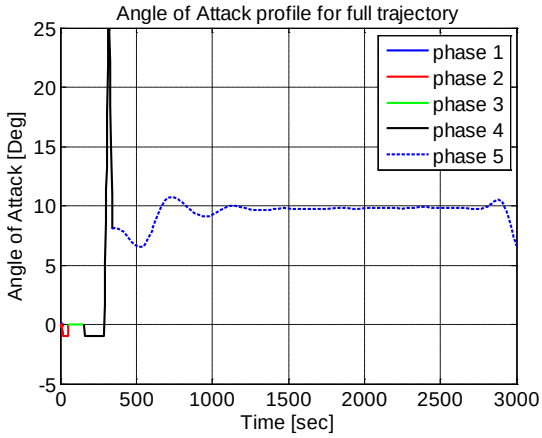

Figure 39 Angle of Attack profile for full path trajectory

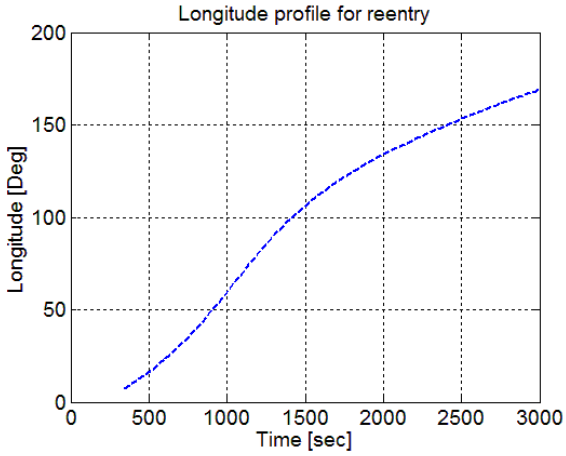

Figure 42 Longitude profile for full path trajectory

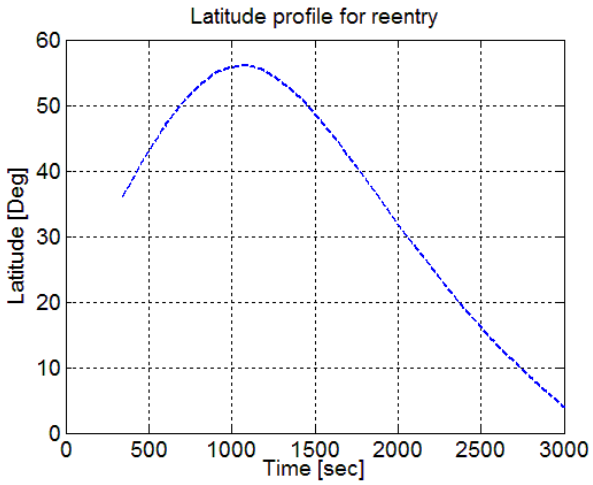

Figure 43 Latitude profile for full path trajectory

X. Fifth Case Study for Min Velocity

The objective function in Fifth case study is min velocity at the reentry phase for full trajectory with suppressing the oscillations in the range profile; the next Table 4 represents the different constraints at the initial and final points

Table 4 Initial and Final constraints for min velocity

Parameter	Symbol	Initial value	Symbol	Final value
Height	r_0	70000 m	r_f	Free
Longitude	θ_0	0°	θ_f	Free
Latitude	φ_0	0°	φ_f	4°
Velocity	V_0	6900 m /s	$\mathbf{V_f}$	**Min**
Flight path angle	γ_0	0°	γ_f	0°
Azimuth angle	ψ_0	65°	ψ_f	Free
Angle of attack	α_0	Free	α_0	Free
Bank angle	σ_0	Free	σ_f	Free

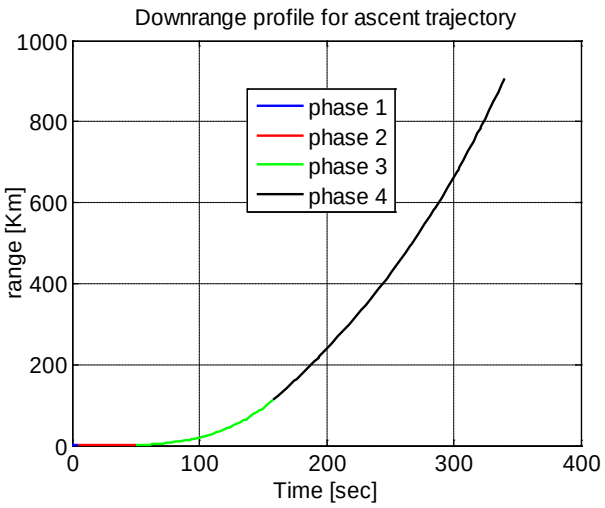

Figure 44 Range profile for full path trajectory

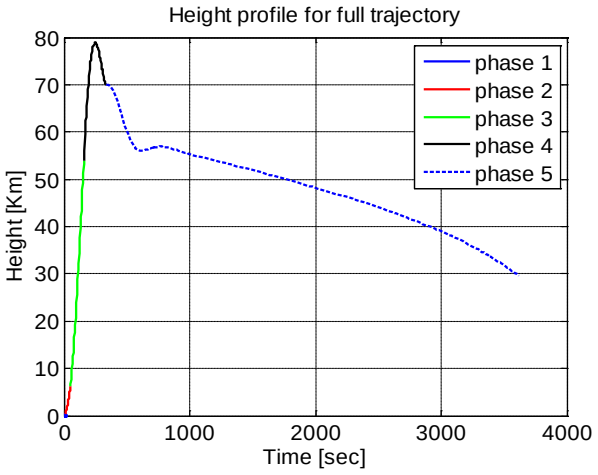

Figure 45 Height profile for full path trajectory

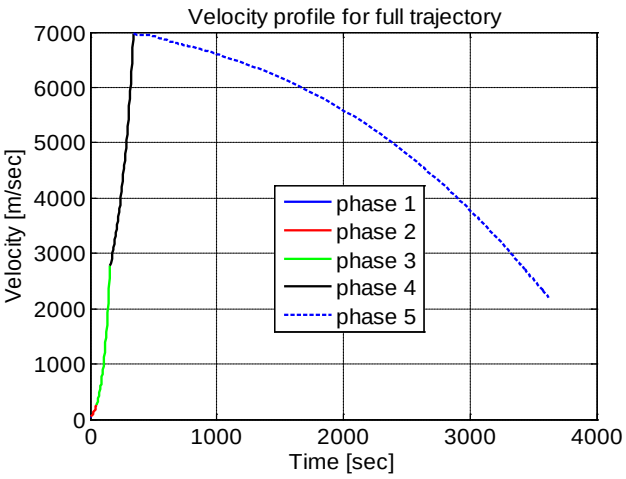

Figure 46 Velocity profile for full path trajectory

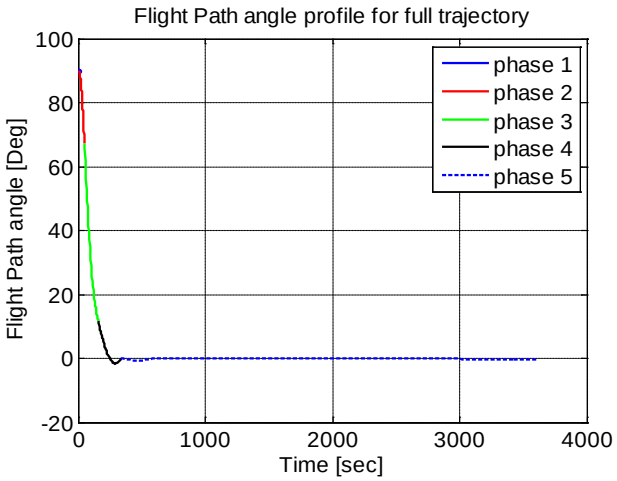

Figure 47 Flight path angle profile for full path trajectory

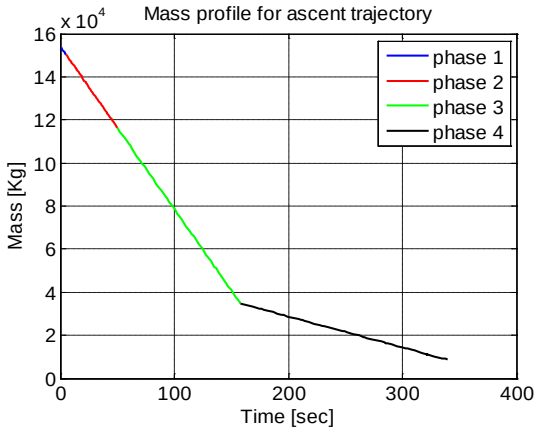

Figure 48 Mass profile for full path trajectory

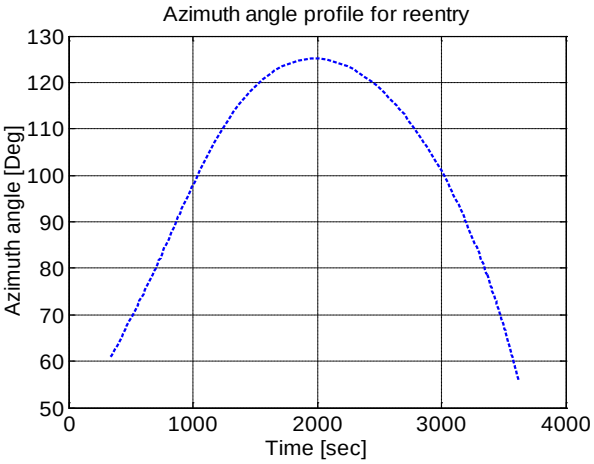

Figure 49 Azimuth angle profile for full path trajectory

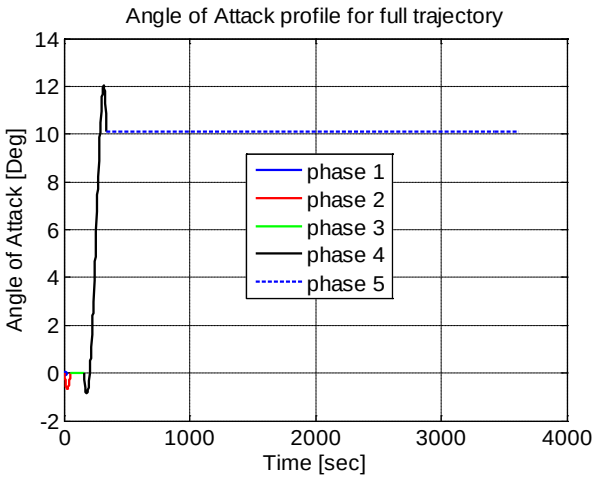

Figure 50 Angle of attack profile for full path trajectory

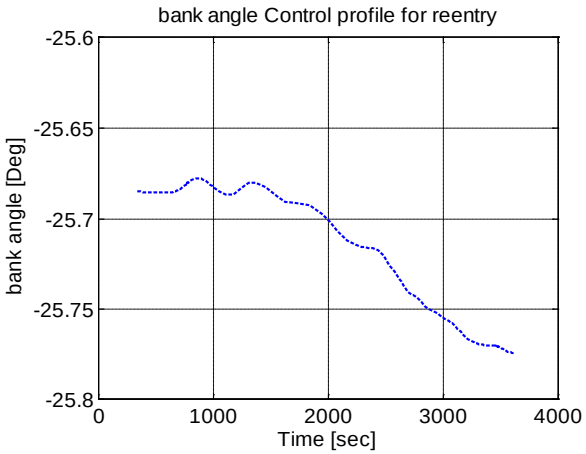

Figure 51 bank angle profile for full path trajectory

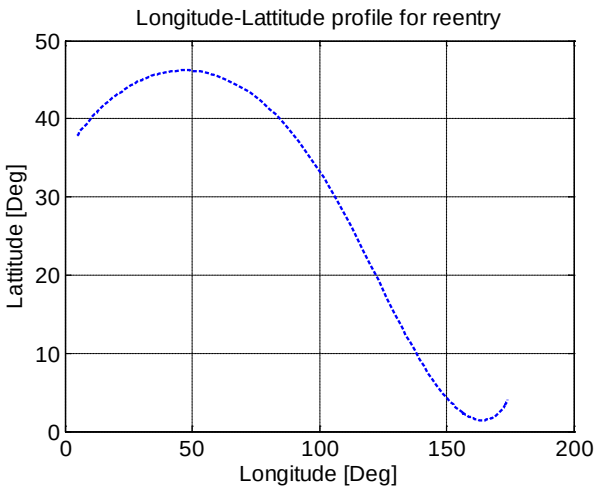

Figure 52 Longitude-Latitude profile for full path trajectory

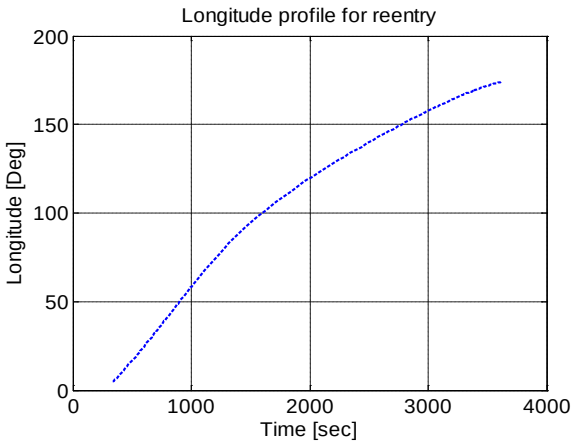

Figure 53 Longitude profile for full path trajectory

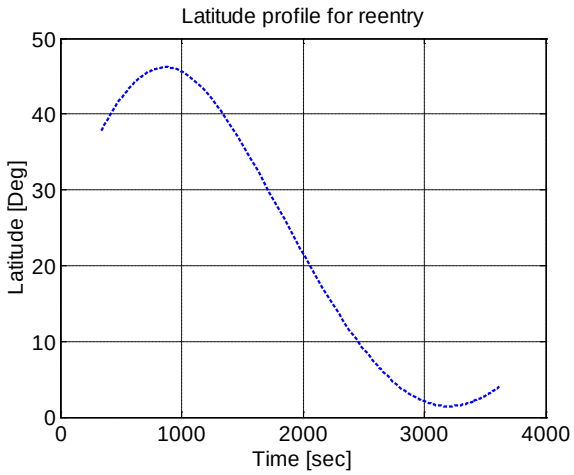

Figure 54 Latitude profile for full path trajectory

XI. Conclusion

One of the most interesting and challenging problem areas for high-speed air-vehicle is that trajectory optimization. Most of previous work concentrated only for separate phase. In this paper introduced the trajectory optimization for double phase -ascent and glide phases- for different vehicles. Tittan II dynamics used in ascent phase while CAV-H dynamics used in gliding phase also, how to initiate the final constraints for the ascent to meet the initial requirements for the gliding phase to link the two phase with each other. Finally complete analysis for full trajectory for different final gliding constraints to insure the performance and suitable for different problems.

References

[1] Kirk, D., Optimal Control Theory An Introduction, Dover Publications Inc., Mineola, New York, 2004.

[2] Schleich, W., "The Space Shuttle ascent guidance and control", Guidance and Control Conference, San Diego,CA,U.S.A., 1982.

[3] Ma, L., Shao, Z., Chen, W., Lv, X., Song, Z., "Three-Dimensional Trajectory Optimization for Lunar Ascent Using Gauss Pseudospectral Method", AIAA Guidance, Navigation, and Control Conference, San Diego, California, USA, 2016.

[4] Rahman, T., Hao, Z., "Trajectory Optimization of Hypersonic Vehicle using Gauss and Legendre Pseudospectral Method", International Conference on Mechanical and Electrical Technology, Dalian, China, 2011.

[5] Fariba, F., Ross, I., "Trajectory optimization by indirect spectral collocation methods", Astrodynamics Specialist Conference, Denver, CO, U.S.A., 2000.

[6] Paluszek, MA., Thomas, SJ., "Trajectory Optimization Using Global Methods", The 29th International Electric Propulsion Conference, Princeton University, 2005.

[7] Huang, G., Lu, Y., Nan, Y., "A survey of numerical algorithms for trajectory optimization of flight vehicles", Sci. China Technol. Sci.,Vol. 55, Issue 9, 2012, pp. 2538.

DOI:10.1007/s11431-012-4946-y.

[8] Garg, D., " Advances in Global Pseudospectral Methods for Optimal Control",thesis, University of Florida, 2011.

[9] Lin, M., Chen, W., Zhengy, S., Zhi, J., "A unified trajectory optimization framework for lunar ascent", Advances in Engineering Software Vol. 94, 2016, pp. 32-45.

[10] Benson, D., "A Gauss Pseudospectral Transcription for Optimal Control", Thesis, Massachusetts Institute of Technology, 2005.

[11] Xu, H., Wanchun, C., "An Energy Management Ascent Guidance Algorithm" 17th AIAA International Space Planes and Hypersonic Systems and Technologies Conference, San Francisco, California, 2011.

[12] Da, Z., Xuefang, L., Liu, L., Wang, Y., "An Online Ascent Phase Trajectory Reconstruction Algorithm Using GPM", Modelling Identification and Control, Wuhan, China 2012.

[13] Lu, P., Zhang, L., Sun, H., "Ascent Guidance for Responsive Launch: A Fixed-Point Approach", AIAA Guidance, Navigation, and Control Conference and Exhibit, San Francisco, California 2005.

[14] Dukeman, G., "Atmospheric Ascent Guidance for Rocket-Powered Launch Vehicles", AIAA Guidance, Navigation, and Control Conference and Exhibit, Monterey, California 2002.

[15] Zhang, K., Chen, W., "Reentry Vehicle Constrained Trajectory Optimization", 17th AIAA International Space Planes and Hypersonic Systems and Technologies Conference, San Francisco, California 2011.

[16] Lu, P., "Entry Guidance: A Unified Method", Journal of Guidance, Control, and Dynamics, Vol. 37, 2014.

[17] Hao, Z., Jiafeng, L., Wanchun, C., Rahman, T., "Rapid Entry Trajectories Generation with Multi-Constraints for CAV", 3rd IEEE International Conference on Computer Science and Automation Engineering, Guangzhou, China 2013.

[18] Gräßlin, M., Telaar, J., Schöttle, U., "Ascent and reentry guidance concept based on NLP-methods", Acta Astronautica, Vol. 55, 2004, pp. 461-71.

[19] Rahman, T., "Design of Guidance Method for Multiple Phases of Hypersonic Vehicle Flight", Thesis, Beihang University, Beijing, China, 2014.

[20] Linshu, H. "Solid Ballistic Missile Design", Beihang University, Beijing, China, 2004.

[21] Yang, L., Chen, W., Liu, X., Zhou, H., "Steady Glide Dynamic Modeling and Trajectory Optimization for High Lift-to-Drag Ratio Reentry Vehicle", International Journal of Aerospace Engineering, Vol. 2016, 2016, pp. 1-14.

[22] Phillips, T., "A common aero vehicle CAV model description and employment guide", Report, Schafer Corporation For AFRL and AFSPC 2003.

[23] Yi, H., Wanchun, C., "Trajectory Optimization of a cruise missile using the Gauss Pseudospectral Method" Control and Decision Conference (2014 CCDC), The 26th Chinese Changsha IEEE, 2014, pp. 652 - 7.

DOI: 10.1109/CCDC.2014.6852247

[24] Patterson, M., Rao, A., "A General-Purpose Matlab Toolbox for Solving Optimal Control Problems Using the Radau Pseudospectral Method", Report, University of Florida, 2013.